Separating Metabolite Contribution from Multiple CEST Pools at 7T

THESIS

submitted in partial fulfillment of the
requirements for the degree of

MASTER OF SCIENCE
in
PHYSICS

Author :	Jaimy Plugge
Student ID :	s1654845
Supervisor :	Dr. Jan-Willem Beenakker
	Dr. Ir. Ece Ercan
2^{nd} corrector :	Dr. Lucia Bossoni

Leiden, The Netherlands, August 23, 2020

Separating Metabolite Contribution from Multiple CEST Pools at 7T

Jaimy Plugge

Huygens-Kamerlingh Onnes Laboratory, Leiden University
P.O. Box 9500, 2300 RA Leiden, The Netherlands

August 23, 2020

Abstract

In this thesis, the potential of Chemical Exchange Saturation Transfer to image brain metabolites is presented. The Bloch-McConnell equations are simulated and the optimal parameters are found to be $3.5\mu T$, $t_{sat} = 1s$ for glutamate and $3\mu T$, $t_{sat} = 1.5s$ for creatine. Furthermore, multiple quantification methods, including MTR asymmetry, Lorentzian fits and spinlock fits are evaluated for quantifying CEST signal from glutamate and creatine. The quantification methods are tested on the Bloch-McConnell simulations, 2-pool phantoms, 3-pool phantoms and *in vivo*.

Contents

Version of August 23, 2020– Created August 23, 2020 - 13:21

1 Introduction

With almost 900.000 MRI exams[1] every year and about 226 MRI units[2] in The Netherlands, Magnetic Resonance Imaging (MRI) has proven to be a mainstay in medical examination, being a non-invasive imaging technique. MRI is able to obtain high soft tissue contrast without the use of ionizing radiation.

Besides providing anatomical images, MRI can also be used to study brain metabolism. Two metabolites this thesis will focus on are glutamate and creatine. Glutamate is an excitatory neurotransmitter which plays a central role in learning, memory and cognition[3]. Lowered glutamate levels have been observed in neurological disorders such as Alzheimer Disease, Schizophrenia etc.[4]. Creatine is a substrate and product of the energy production inside the body, as it is used as a buffer for the phosphate group in Adenosine triphosphate (ATP). The brain is a very active organ of billions of neurons. Due to its high activity, it has a high demand for energy[5]. This high demand makes creatine an interesting factor in brain health.

Evidently, it is important to image glutamate and creatine levels in the brain. However, with normal MRI it is not possible to image metabolite levels, since the Larmor frequency of their ^1H protons is very close to that of water. Due to the abundance of water in the brain, the obtained MRI signal is dominated by the water signal. This makes it hard to separate the metabolite signal from the water signal. Another MRI technique which makes use of water suppression methods has to be found.

1.1 Magnetic Resonance Spectroscopy

Magnetic Resonance Spectroscopy (MRS) is a technique that makes use of water suppression methods like *inversion recovery* or *chemical shift selective*. After the water suppression, a 90 degree pulse is applied at the resonance

Version of August 23, 2020– Created August 23, 2020 - 13:21

frequency of the target metabolite. After this pulse, the Free Induction Decay (FID) is obtained of which a Fourier transform is taken (see figure 1.1). After the FID, the tissue needs at least 5 times its T_1 time to recover

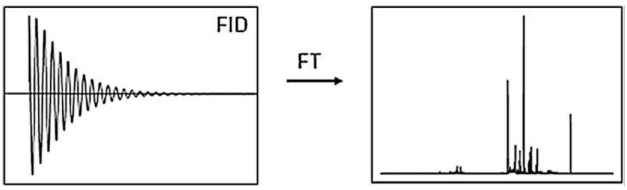

Figure 1.1: *[6] Free Induction Decay and its Fourier Transform.*

to 99% of its initial magnetization. But since the amount of metabolites is very low, the signal of multiple FIDs need to be taken and averaged. This results in long scan times since each measurement takes several T_1 times to obtain a sufficient SNR. Furthermore, due to the low amount of the metabolites, bigger voxel sizes need to be used to obtain enough signal which results in a low resolution. This low resolution makes it hard to differentiate between for example the glutamate levels in grey and white matter[7]. Most *in vivo* voxel sizes in MRS are about $20mm^3$[4] compared to about $1mm^3$ in conventional MRI.

1.2 Chemical Exchange Saturation Transfer

The term Chemical Exchange Saturation Transfer (CEST) was first proposed by Ward et al.[8] in 2000 and is already used to image amide levels.

CEST makes use of the spontaneous exchange of ^1H to achieve water saturation. In MR experiments, the signal is proportional to the difference between protons in the *parallel* and the *anti-parallel* state when a B_0-field is present. Since the parallel state is energetically more favorable, more protons will be in that state, see figure 1.2. Since the signal in MRI is proportional to this difference, no signal is obtained when both energy levels are occupied by the same amount of protons. This is called saturation, a substance can be saturated by adding exactly enough energy to some of the spins to excite from the parallel to the anti-parallel state which in MR is achieved by an RF pulse. When a tissue is saturated, no MR signal will be obtained from that tissue as long as it is saturated. Saturation is not the equilibrium state of the tissue inside the magnetic field, as it is more energetically favorable for the protons to be in the parallel state. So some of the anti-parallel spins inside the saturated tissue will "decay" to the parallel state which depends on the relaxation time T_1.

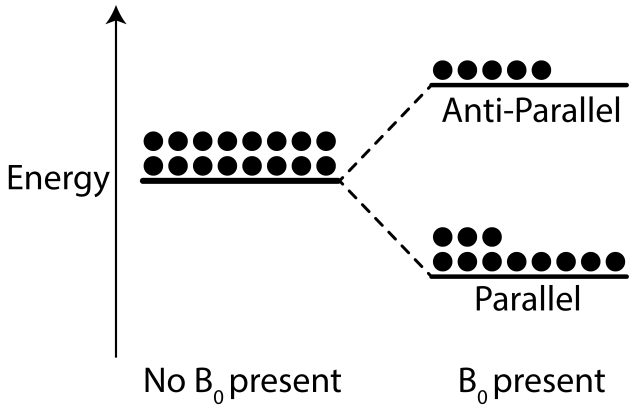

Figure 1.2: *Schematic representation of proton energy configuration.*

In CEST experiments, an RF pulse is applied to the metabolite to saturate its hydrogen proton (^1H), see figure 1.3. Due to spontaneous exchange, the saturated ^1H will move to the water pool and decrease the total magnetization of the water while the metabolite will receive an unsaturated ^1H. The unsaturated ^1H will be saturated by the still present RF pulse and exchange with the ^1H of another water molecule. This will happen 10^2 to 10^3 times a second due to the high exchange rate of the metabolites. With n exchanges, the detectability of the metabolite is improved n times.

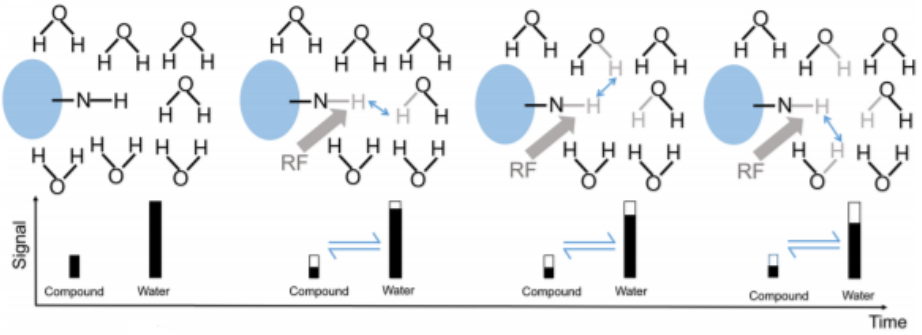

Figure 1.3: *[4] This figure shows global idea of CEST, the bar depicts the maximum amount of signal able to be obtained from the substance and the hollow bar depicts the reduced signal due to saturation.*

Multiple CEST pools will be discussed in this thesis, figure 1.4 shows the effect of these different CEST pools on the Z-spectrum. Amides are found at $3.5ppm$ on the Z-spectrum, amide CEST (commonly called APT)

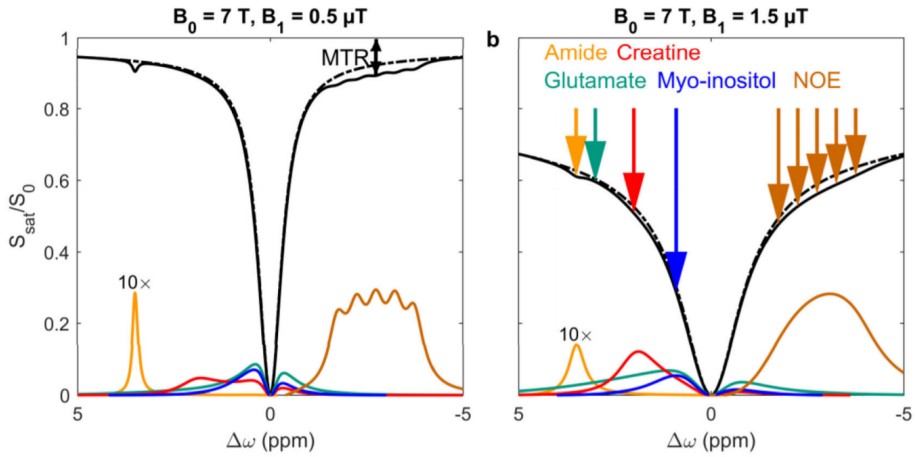

Figure 1.4: *[9] Different CEST pools and their effect on the Z-spectrum.*

is the most widely used CEST imaging[4]. Glutamate is found at $3ppm$, creatine at $2ppm$ and Myo-Inositol at $1ppm$ on the Z-spectrum. On the negative frequency side of the Z-spectrum, NOE is found. The MT effect shifts the Z-spectrum down as a function of B_1 strength, which is also shown in figure 1.4.

1.3 This Thesis

CEST has mainly been used in the literature to image amide proteins. A new CEST direction includes metabolite weighted CEST images. However, these studies are at the initial stage and further research needs to be done to evaluate the potential of metabolite weighted CEST images. To quantify the signal in metabolite CEST and separate the overlapping signal of the metabolites still remain a challenge. This thesis elaborates on our progress towards the separation of glutamate and creatine.

Chapter 2, *Theory*, will describe the Bloch-McConnell equations which describe a simplified model of CEST experiments. Furthermore, the Nuclear Overhauser effect and Magnetization Transfer, two effects that need to be taken into account while doing CEST experiments, are explained. Chapter 3, *Methodology*, describes the simulation and multiple ways to quantify the CEST signal are discussed. In chapter 4, *Results*, the results from simulation, phantom data and in vivo data are presented. The results are discussed in chapter 5, *Discussion*, where the future directions are also described. The conclusion from these experiments can be found in chapter 6, *Conclusion*.

2 Theory

In this chapter, a simplified model for CEST is introduced and the Bloch-McConnell equations that describe this model are shown and explained. Furthermore, signal in CEST is explained and the optimal scan parameters for glutamate and creatine are shown.

2.1 Bloch-McConnell Equations

The assumptions made for the simplified CEST 2-pool model are shown in a schematic in figure 2.1. Pool a is the pool consisting of water and pool b consists of the metabolite of interest. Pool a is much bigger than pool b and the fraction of pool b to pool a is given by $MB = \frac{\text{Amount pool } b}{\text{Amount pool } a}$ which is assumed to be much less than 1 ($MB \ll 1$). The rate of exchange from pool b to pool a is given by C_b and the exchange from pool a to pool b is given by $C_a = MB \cdot C_b$. The Bloch-equations with the added interaction terms are called the Bloch-McConnell equations.

The Bloch-McConnell equations describe the change in magnetization M of the spins of both (water and CEST) pools in cartesian coordinates,

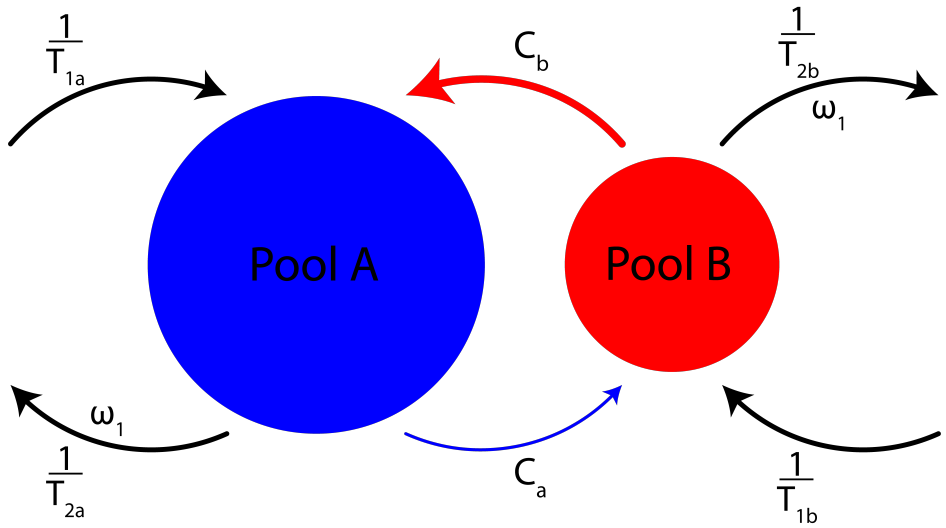

Figure 2.1: *The simplified two pool model. Pool χ loses magnetisation from $T_{2\chi}$ and the irradiated RF $B_1 = \frac{\omega_1}{\gamma}$, it gains magnetisation from its $T_{1\chi}$ relaxation. Furthermore, they exchange magnetisation due to C_a and C_b.*

they are given by[10]:

$$\begin{aligned}
\frac{dM_x^a}{dt} &= -(\omega - \omega_a)M_y^a - k_{2a}M_x^a + C_b M_x^b \\
\frac{dM_y^a}{dt} &= (\omega - \omega_a)M_x^a - k_{2a}M_y^a + C_b M_y^b + \omega_1 M_z^a \\
\frac{dM_z^a}{dt} &= \frac{M_0^a}{T_{1a}} - k_{1a}M_z^a + C_b M_z^b - \omega_1 M_y^a \\
\frac{dM_x^b}{dt} &= -(\omega - \omega_b)M_y^b - k_{2b}M_x^b + C_a M_x^a \\
\frac{dM_y^b}{dt} &= (\omega - \omega_b)M_x^b - k_{2b}M_y^b + C_a M_y^a + \omega_1 M_z^b \\
\frac{dM_z^b}{dt} &= \frac{M_0^b}{T_{1b}} - k_{1b}M_z^b + C_a M_z^a - \omega_1 M_y^b
\end{aligned} \tag{2.1}$$

Here, ω_χ is the Larmor frequency of pool $\chi \in \{a, b\}$, ω is the frequency range along which we describe these equations. $k_{\eta\chi} = T_{\eta\chi}^{-1} + C_\chi$ with $\eta \in \{1, 2\}$ and $T_{\eta\chi}$ the relaxation time of pool χ. C_χ is the rate of transition of spins leaving pool χ and ω_1 is given by $\omega_1 = 2\pi B_1$, with B_1 the strength of the RF radiation. M_0^χ is the magnetisation of the spins in the z-direction before the RF pulse.

2.2 Saturation Efficiency

The signal in CEST is linearly proportional to the saturation efficiency α [11] and is defined by[12]

$$\alpha \approx \frac{(\gamma B_1)^2}{(\gamma B_1)^2 + pq} \quad . \tag{2.2}$$

Here, we have the terms

$$p = \frac{1}{T_{2b}} + C_b - \frac{C_b C_a}{\frac{1}{T_{2a}} + C_a} \tag{2.3}$$

and

$$q = \frac{1}{T_{1b}} + C_b - \frac{C_b C_a}{\frac{1}{T_{1a}} + C_a} \quad . \tag{2.4}$$

Formula 2.2 shows that the saturation efficiency depends on the B_1 pulse and the exchange rate. To quantitatively discuss the effect of the exchange rate on the saturation efficiency, 2 regimes have to be discussed, $pq \ll \gamma B_1$ and $pq \gg \gamma B_1$. $pq \ll \gamma B_1$ yields $\alpha \approx 1$ for every B_1. But for $pq \gg \gamma B_1$, $\alpha \approx \frac{(\gamma B_1)^2}{pq}$ which corresponds to $\alpha \approx 0$. This formula will thus make a transition from $\alpha = 0$ to $\alpha = 1$ as a function of B_1. Figure 2.2 shows that

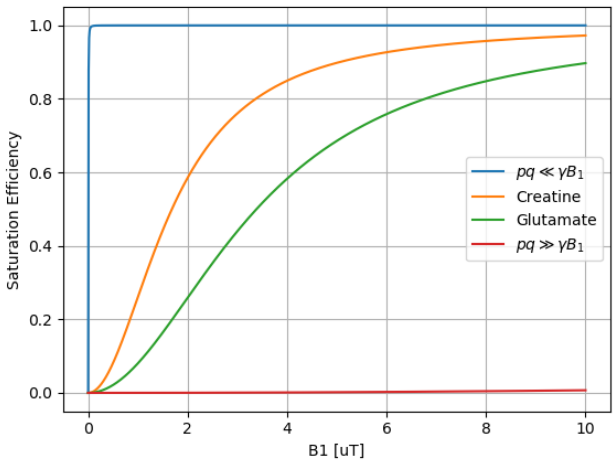

Figure 2.2: *Effect of exchange rate on the saturation efficiency for the case of $pq \ll \gamma B_1$, Creatine, Glutamate and $pq \gg \gamma B_1$*

glutamate would need a higher B_1 to obtain the same amount of saturation efficiency (and thus signal) as creatine.

Version of August 23, 2020– Created August 23, 2020 - 13:21

Furthermore, saturation time is also a parameter in the experiments. Saturation time is defined as the time taken to saturate the protons of the metabolite and is effectively the time of the B_1-pulse. Longer saturation time corresponds to more time for the protons to exchange with water, but also more time for the water protons to relax back into their equilibrium configuration. This results in an optimum saturation time for different metabolites since the exchange rate is different for different metabolites. Faster exchanging metabolites like glutamate benefit from shorter saturation times since they have already exchanged a lot of their protons before the water is relaxed back. Slower exchanging metabolites like creatine benefit from longer saturation times due to them not reaching an optimum amount of saturation in the same time as faster exchanging metabolites do. So a higher scan efficiency for glutamate is expected for high B_1 and short saturation time. But creatine will achieve its highest scan efficiency for lower B_1 and longer saturation time, this also corresponds to what is found from the simulations (see figure 2.3).

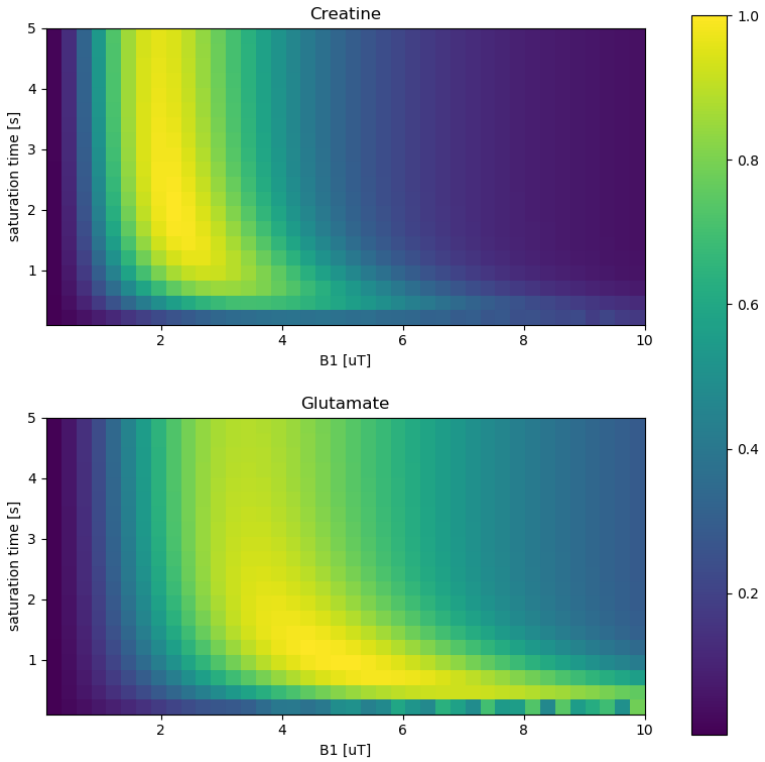

Figure 2.3: *An optimisation map for both creatine and glutamate, made from the simulation. Both optimisation maps are normalized.*

2.3 Nuclear Overhauser Effect and Magnetization Transfer

As already explained in section 1.2, in CEST, the saturation is transferred between molecules due to the physical exchange between the protons. But this is not the only way saturation can be transferred, two dipolar coupled neighboring protons can also transfer their saturation. When two spins are coupled (figure 2.4), after saturating spin A, cross relaxation between spin A and spin B causes the saturation of spin A to be transferred to spin B. After T_1 relaxation, both spins are in their equilibrium configuration. This effect is called Nuclear Overhauser Effect (NOE). Notice that this cross relaxation has to be faster than the T_1 time, since otherwise spin A is already relaxed before it can transfer its saturation to spin B. In CEST experiments,

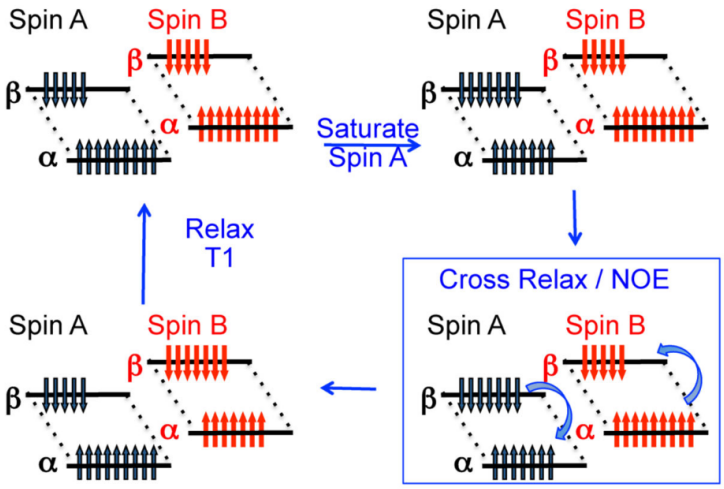

Figure 2.4: *[9] Two spin pools A and B which are dipolar coupled can transfer their saturation.*

NOE is shown in the Z-spectrum in the negative frequency region, see figure 2.5. This is caused by a saturated proton in a molecule in which the saturation is transfered through the backbone of the molecule due to bipolar coupling and eventually chemically exchanged with water. This is specifically called NOE-relayed (rNOE)[9].

Dipolar coupling can also take place between semi-solid tissue components and water. Semi-solids have very short T_2 times which corresponds to a very broad peak in the Z-spectrum. So even when a resonance pulse is applied far from water, it can partially saturate the semi-solids which can due to dipolar coupling (partially) saturate the water[9]. This effect is

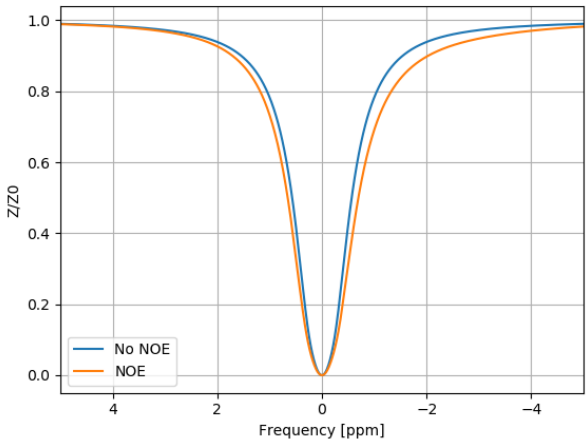

Figure 2.5: *Z-spectrum with and without NOE effect,* $B_1 = 1\mu T$ *and saturation time is* $1s$.

referred to as Magnetization Transfer and its effect on the Z-spectrum is shown in figure 2.6.

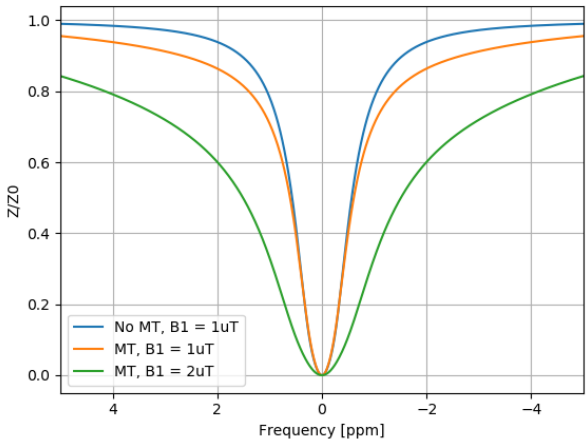

Figure 2.6: *Z-spectrum with and without MT effect, the saturation time is* $1s$.

3 Methodology

This chapter will first explain how the simulation was constructed from the Bloch-McConnell equations and how a Z-spectrum is obtained from these simulations. The simulations will be used in this thesis to optimize the CEST parameters. Next, the different methods to quantify the signal from the Z-spectrum like MTR asymmetry are discussed. Last, the construction of the phantoms and the experiment parameters are presented.

3.1 CEST simulation

The Bloch-McConnell equations correspond to the expected signal after the CEST. First, the simulation for the 2-pool model will be described. At the end of this section, the method to expand to multiple pools is explained. To obtain the analytical solution, let us start by writing equation 2.1 as a vector matrix equation:

$$\frac{d}{dt}\begin{pmatrix} M^a \\ M^b \end{pmatrix} = \begin{pmatrix} K_a & L_b \\ L_a & K_b \end{pmatrix}\begin{pmatrix} M^a \\ M^b \end{pmatrix} + \begin{pmatrix} X_0^a \\ X_0^b \end{pmatrix} \tag{3.1}$$

with

$$K_\chi = \begin{pmatrix} -k_{2\chi} & -(\omega-\omega_\chi) & 0 \\ (\omega-\omega_\chi) & -k_{2\chi} & -\omega_1 \\ 0 & \omega_1 & -k_{1\chi} \end{pmatrix} \tag{3.2}$$

$$L_\chi = C_\chi \cdot \mathbb{1} \tag{3.3}$$

$$M^\chi = \begin{pmatrix} M_x^\chi \\ M_y^\chi \\ M_z^\chi \end{pmatrix} \tag{3.4}$$

$$X_0^\chi = \begin{pmatrix} 0 \\ 0 \\ \frac{M_0^\chi}{T_{1\chi}} \end{pmatrix} \tag{3.5}$$

Here, ω_χ is the Larmor frequency of pool $\chi \in \{a, b\}$, ω is the frequency range along which we describe these equations. $k_{\eta\chi} = T_{\eta\chi}^{-1} + C_\chi$ with $\eta \in \{1, 2\}$ and $T_{\eta\chi}$ the relaxation time of pool χ. C_χ is the rate of transition of spins leaving pool χ and ω_1 is given by $\omega_1 = 2\pi B_1$, with B_1 the strength of the RF radiation. M_0^χ is the magnetisation of the spins in the z-direction before the RF pulse.

With the Bloch-McConnell equations in the vector matrix equation form $\frac{d}{dt}\vec{M} = A\vec{M} + \vec{X}$, they can solved for $\vec{M}$. This is a linear differential equation with solution

$$\vec{M}(t) = \lambda e^{A \cdot t} - A^{-1}\vec{X} \quad , \tag{3.6}$$

with λ a constant bounded by the initial condition $\vec{M}(0) \equiv M_0$. This initial condition yields $\lambda = \vec{M}_0 + A^{-1}\vec{X}$. The formal solution[13] to the Bloch-McConnell equations is found after setting $t = t_{sat}$:

$$\vec{M} = \exp(A \cdot t_{sat})(\vec{M}_0 + A^{-1}\vec{X}) - A^{-1}\vec{X} \quad . \tag{3.7}$$

The saturation time t_{sat} is the duration of the B_1 pulse. In MR, only the z-magnetization of the protons yields signal. So from this vector $\vec{M}$, the only interesting components are the z-components of both pools. After the M_z-components of both pools are added for every frequency ω and plotted, the so called Z-spectrum is obtained (figure 3.1).

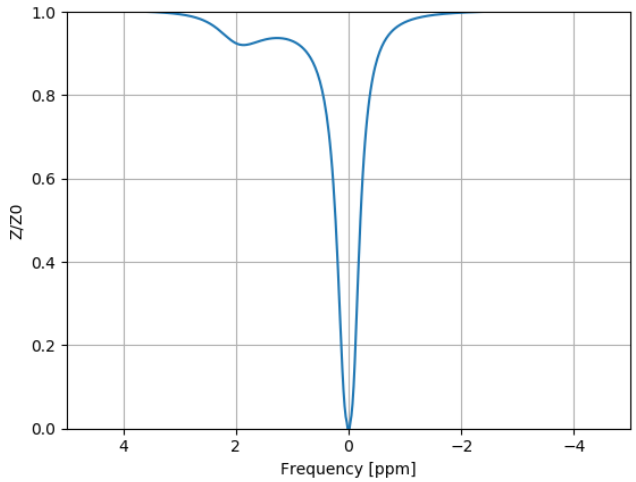

Figure 3.1: *An example of a Z-spectrum, simulation data of* $40mM$ *creatine,* $7T$*,* $B_1 = 0.5\mu T$ *and* $1s$ *saturation time.*

Until this point we only discussed 2 pools, but we may want to look at multiple metabolites in water. First, we need to assume that the metabo-

lites do only exchange ^1H with water and not with each other, which is plausible due to their low concentration. The matrix equations from equation 3.1 can than easily be expanded to a 3-pool model:

$$\begin{pmatrix} K_a & L_{ba} & L_{ca} \\ L_{ab} & K_b & 0 \\ L_{ac} & 0 & K_c \end{pmatrix} \begin{pmatrix} M^a \\ M^b \\ M^c \end{pmatrix} = - \begin{pmatrix} X_0^a \\ X_0^b \\ X_0^b \end{pmatrix} \tag{3.8}$$

Here, K and L are the same as in equation 3.2 and 3.3 respectively, with now $\chi \in \{a, b, c\}$ and $C_a = C_{ab} + C_{ac}$. The exchange rates $C_{\chi\chi'}$ now denote the exchange from pool χ to χ'. Adding another pool just adds 3 more rows and columns to these matrices, this way the model can be expanded for n pools.

3.1.1 Simulating a Semi-Solid MT Pool

Another pool that can be added to the simulation, is a semi-solid MT pool. The difference between CEST pools and semi-solid MT pools are the very short T_2 times of the MT pools ($\sim 10^{-5}s$). Due to these short T_2 times, only the z-magnetization needs to be taken into account. So for only water and MT, this results in $\vec{M} = (M_x^a, M_y^a, M_z^a, M_z^{MT})^T$. The matrix A from the Bloch-McConnell equation now becomes[14]

$$\begin{pmatrix} -\frac{1}{T_{2a}} & -(\omega - \omega_a) & 0 & 0 \\ (\omega - \omega_a) & -\frac{1}{T_{2a}} & -\omega_1 & 0 \\ 0 & \omega_1 & -k_{1a} & C_{MT} \\ 0 & 0 & C_{MT} & -k_{1MT} - R_{rfc} \end{pmatrix} \quad , \tag{3.9}$$

with ω_a the Larmor frequency of pool a, ω is the frequency range along which we describe these equations. $k_{1\chi} = T_{1\chi}^{-1} + C_\chi$ with $\chi \in \{a, MT\}$ and $T_{1\chi}$ the relaxation time of pool χ. C_{MT} is the rate of transition of spins the semi-solid pool and ω_1 is given by $\omega_1 = 2\pi B_1$, with B_1 the strength of the RF radiation.

$$R_{rfc} = \omega_1 \pi g_c(\omega) \quad , \tag{3.10}$$

with

$$g_c(\omega) = \int_0^{\frac{\pi}{2}} d\theta \sin(\theta) \sqrt{\frac{2}{\pi}} \frac{T_{2MT}}{|3\cos^2\theta - 1|} \cdot \exp\left[-2\Big(\frac{2\pi\omega T_{2MT}}{|3\cos^2\theta - 1|} \Big)^2 \right] \quad . \tag{3.11}$$

3.2 CEST quantification

Multiple ways of CEST quantification have been proposed, of which a few will be discussed here. The easiest method would be to look at the dip around the right frequency value and define the signal to be $1 - Z/Z0(\omega_b)$. The problem with this method is that it also may include some signal from the water and MT since its peak may overlap at the frequency value of interest.

3.2.1 MTR asymmetry

To get rid of this potential water overlap, a common method is to make use of the expected symmetry of the water signal. Since the CEST effect is asymmetric around the water frequency which in CEST experiments is set to 0 ppm, the positive frequencies $(+\nu)$ can be subtracted from the negative frequencies $(-\nu)$ with respect to the water frequency. The remaining signal is called the MTR asymmetry and is defined by

$$\mathrm{MTR}_{asym} = \frac{Z_{-\nu} - Z_{+\nu}}{Z_0} \quad , \tag{3.12}$$

calculating the MTR asymmetry for the Z-spectrum of figure 3.1 yields the orange spectrum in figure 3.2. The expected asymmetry of the CEST effect

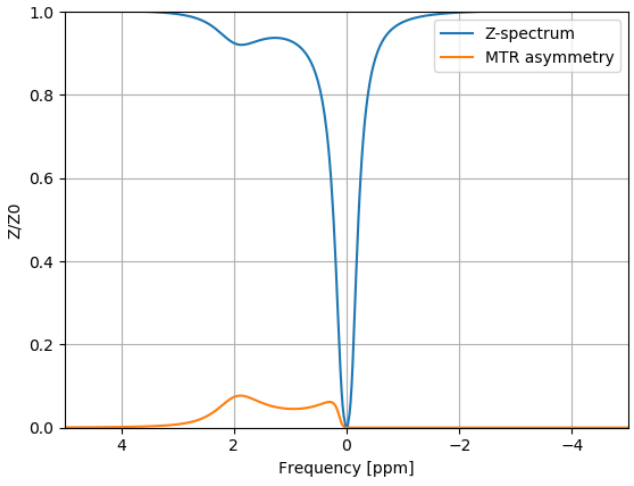

Figure 3.2: *An example of a Z-spectrum with MTR asymmetry, simulation data of* $40mM$ *creatine,* $7T$*,* $B_1 = 0.5\mu T$ *and* $1s$ *saturation time.*

can not always be relied on, since different effects like MT and NOE can negate this asymmetry. Furthermore, this technique is susceptible to B_0 inhomogeneity which can shift the water frequency and yield an asymmetric water signal around 0 ppm. This problem can be mitigated by sampling more around the water frequency and eventually shifting the spectrum to make the dip correspond to 0 ppm.

3.2.2 Lorentzian Fit

Lorentzian fitting to separate signal contribution in CEST already exists in the imaging of amides[15]. For this method, the Z-spectrum is approximated by a sum of Lorentzians of the form

$$S_{lor} = \frac{a}{1 + 4(\frac{\omega - \omega_0}{\gamma})^2} \quad . \tag{3.13}$$

In this formula, a is the height of the peak, ω_0 is the chemical shift of the metabolite and γ is the full width at half maximum (FWHM) of the Lorentzian. To fit the sum of these Lorentzians to our Model of the Bloch-McConnell equations, we use the *least_squares* function from *scipy.optimize* in *Python*. As first guesses for $S_{lor,a}$ for the water pool, we set $a_a = 0.9$ and $\gamma_a = 2\pi(298 \cdot T_{2a})^{-1}$. For the metabolite pool, the first guesses for the least_square function are $a_b = \text{MTR}_{asym}[\omega_b]$ and $\gamma_b = 2\pi(298 \cdot T_{2b})^{-1}$. Here, we used the MTR_{asym} as a first guess, since we expect the actual signal to be close to that value. So for an n-pool model, the amount of fitting parameters for the Lorentzian fit is $2n$ since ω_0 for both pools is at a predetermined value.

3.2.3 Spinlock Fit

Another way to quantify CEST signal, is to find the eigenspace solution of the Bloch-McConnell equations. We will not go far into the derivation of this solution, but for the mathematical background, see the paper from Moritz Zaiss and Peter Bachert[16]. The solution is given by[14]

$$S_{Zaiss} = (\cos^2\theta \cdot Z_i - Z_{ss}) \cdot \exp(-(R_{1\rho} \cdot t_{sat})) + Z_{ss} \quad . \tag{3.14}$$

In this formula, Z_i is the initial magnetization, $\cos^2\theta = \frac{\omega^2}{\omega_1^2 + \omega^2}$, t_{sat} is the saturation time and $R_{1\rho}$ the sum of the contribution from the different pools $R_{1\rho} = R_{\text{eff}} + R_{\text{ex}}^{\text{cest}}$. The contribution from the water pool R_{eff} is given by

$$R_{\text{eff}} = R_{1a}\cos^2\theta + R_{2a}\sin^2\theta \tag{3.15}$$

and the contribution of the metabolite pool

$$R_{\text{ex}}^{\text{cest}} = \frac{\frac{C_a\omega_1^2}{(\omega-\omega_a)^2+\omega_1^2}(\omega_b-\omega_a)^2 + ((\omega-\omega_a)^2+\omega_1^2)\frac{1}{T_{2b}C_b} + \frac{T_{2b}C_b+1}{T_{2b}^2}}{\frac{T_{2b}C_b+1}{T_{2b}C_b}\omega_1^2 + (C_b+\frac{1}{T_{2b}})^2 + (\omega-\omega_b)^2} \quad . \tag{3.16}$$

Z_{ss} is the steady state solution of the Bloch-McConnell equations and is given by[14]

$$Z_{ss} = \frac{\cos^2\theta R_{1obs}}{R_{1\rho}} \quad , \tag{3.17}$$

with $R_{1obs} \approx \frac{1}{T_{1a}}$. The fitting parameters used in the spinlock fit are the concentration of every pool, B_1, $T_{1,\text{water}}$, $T_{2,\text{water}}$ and the fraction of the MT pool ($\frac{\text{Amount MT pool}}{\text{Amount water pool}}$). So for an n-pool model, the amount of fitting parameters is $n+4$ with MT pool and $n+3$ without MT pool.

3.3 Experiments

The phantoms were made by mixing different concentrations of glutamate and/or creatine with purified water. After mixing, the pH of the solutions were measured and some droplets of either *NaOH* or *HCl* were added to get the physiological pH of 7.3. We assumed the addition of the droplets to be too less of a difference for the amount of water to make it negligible.

Both the Phantom Experiments and the In Vivo experiments were done with a $7T$ Achieva Philips whole-body MRI scanner (Philips Healthcare, Best, the Netherlands). The data acquisition for both experiments was done with a 32-channel receive coil (Nova Medical Inc., Wilmington, Massachusetts, USA). The scan parameters are presented in table 3.1.

	Phantom	In Vivo
B_1	0.5 - 4μT	3.5μT
B_1rms	0.42 - 3.32μT	2.92μT
Dynamic Scans	42	42
Offset Range	1.5kHz	1.5kHz
Reference Frequency	300kHz	300kHz
Pulse Duration	50ms	50ms
Pulse Intervals	50ms	50ms
Pulse Repetitions	5 - 25	10
FOV	$246 \times 246mm^2$	$246 \times 246mm^2$
Voxel Size	$1.5 \times 1.5 \times 3mm^3$	$1.5 \times 1.5 \times 3mm^3$
TR	3.7ms	3.7ms
TE	2.0ms	2.0ms
Flip Angle	5°	5°

Table 3.1: *Scan Parameters*

4 Results

This chapter will present the Bloch-McConnell simulation for both glutamate and creatine. The quantification methods are tested for both the simulations and the phantom data. Last, the *in vivo* data is presented and the quantification methods are compared to each other.

4.1 Simulations

This section includes the results for the Bloch-McConnell equations. For the Bloch-McConnell simulation, the Z-spectrum as described in section 3.1 is plotted for both glutamate and creatine. The following Z-Spectra include the MTR asymmetry in orange and will be used to test our fitting methods.

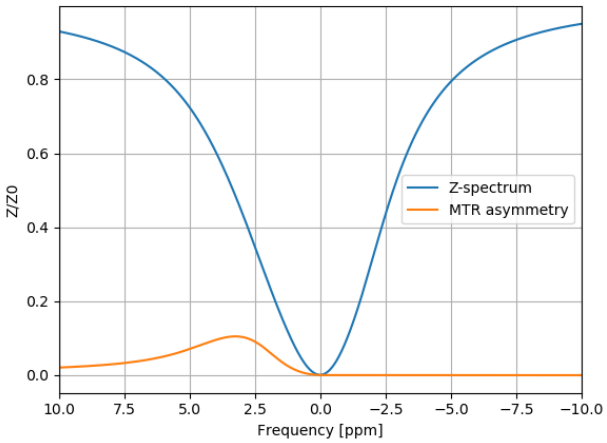

Figure 4.1: *Simulated Z-spectrum of glutamate,* $B_1 = 4\mu T$ *and* $t_{sat} = 2s$.

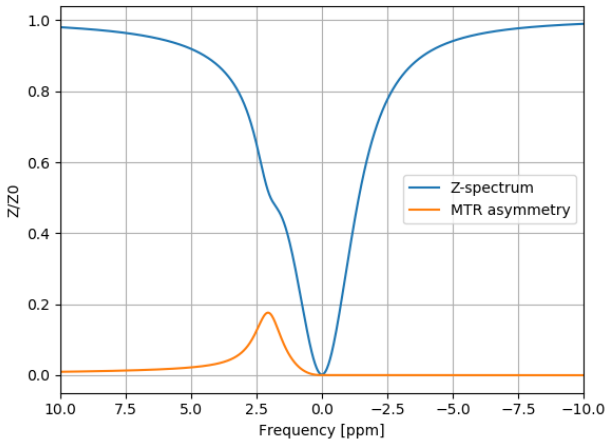

Figure 4.2: *Simulated Z-spectrum of creatine, $B_1 = 2\mu T$ and $t_{sat} = 3s$.*

4.1.1 Optimize CEST Parameters for the Simulations

To obtain the optimal B_1 and t_{sat} for glutamate and creatine, the simulation was repeated for multiple B_1 and t_{sat}. For every parameter, the height of the MTR asymmetry at the resonance frequency of the metabolite was saved to a $2D$-array. After the array was filled in, it was normalized (figure 4.3).

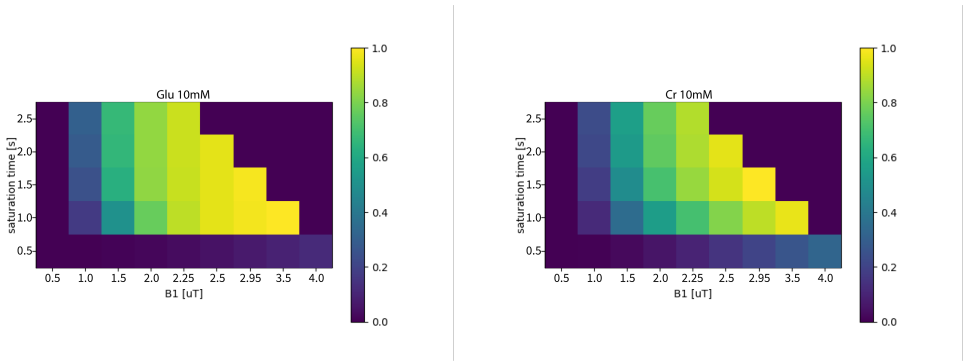

(a) ***(b)***

Figure 4.3: *The normalised optimisation matrices for glutamate (a) and creatine (b). The dark blue pixels in the upper right corner correspond to simulations that were not conducted due to SAR limitations.*

4.1.2 CEST Quantification

In literature, there are multiple methods to quantify the CEST effect, with most of them using the MTR asymmetry. This is the reason why both CEST quantification methods shown here are compared to the MTR asymmetry.

The Lorentzian fits are plotted as $1 - Z$ to make them easier to fit to. They include the Z-spectrum, the Lorentzian fit, the water Lorentzian and the metabolite Lorentzian. Furthermore, the residual is plotted which is defined by $S_{\text{lorentzian}} - (1 - S_{\text{BM simulation}})$. The maximum absolute residual value in these fits was 0.10, of which the data is not shown here.

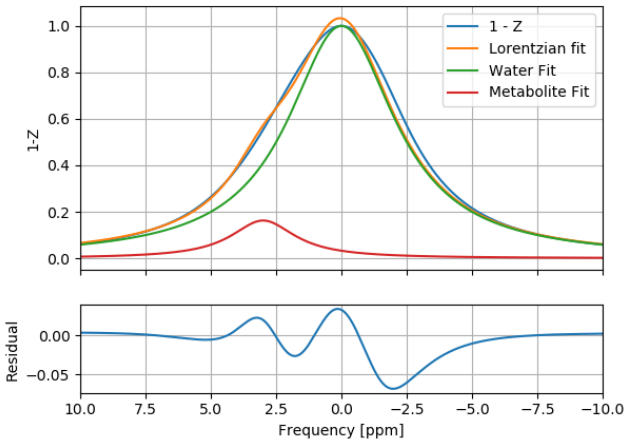

Figure 4.4: *The Lorentzian fit to 1-Z-spectrum, the individual Lorentzians for water and glutamate are plotted in green and red respectively.*

Additionally, the individual metabolite Lorentzians are plotted in figures 4.6 and 4.7 together with the MTR asymmetries from figures 4.1 and 4.2. The individual metabolite Lorentzians correspond to the individual signal one would separate from the data. The MTR asymmetry is used as a comparison due to these simulations being the ideal conditions making them reliable for individual metabolite signal.

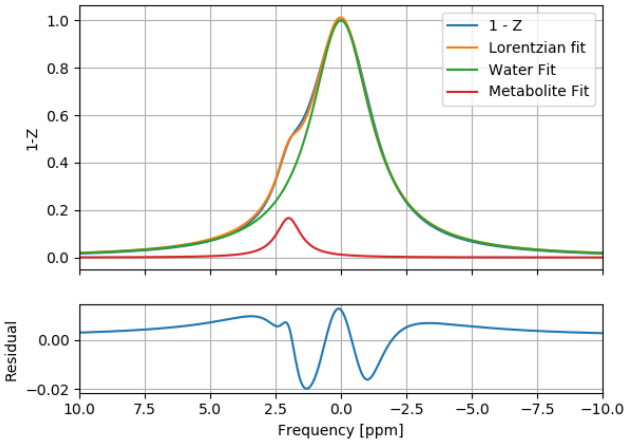

Figure 4.5: *The Lorentzian fit to 1-Z-spectrum, the individual Lorentzians for water and creatine are plotted in green and red respectively.*

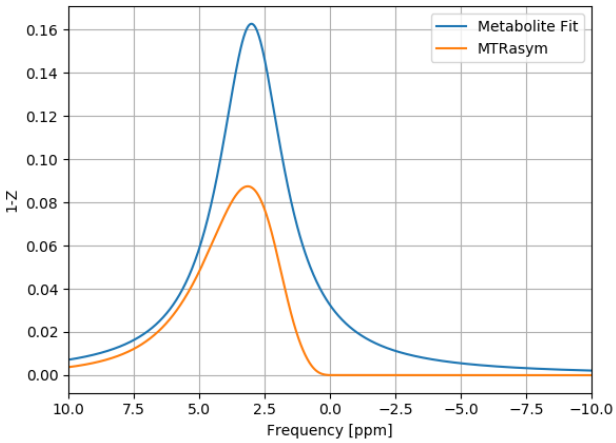

Figure 4.6: *MTR asymmetry together with glutamate Lorentzian fit.*

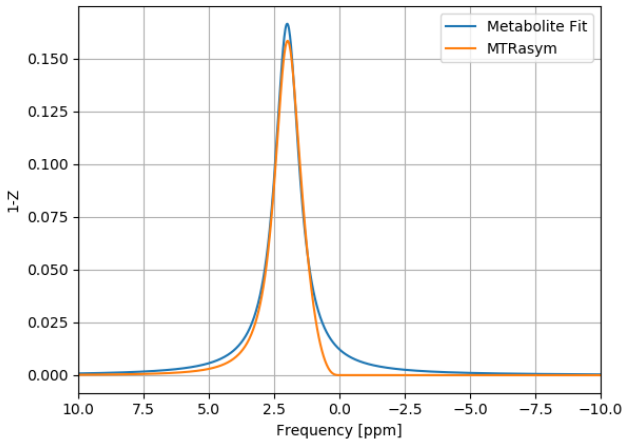

Figure 4.7: *MTR asymmetry together with creatine Lorentzian fit.*

Here, the Bloch-McConnell simulations were fitted by the spinlock fit described in section 3.2.3. These fits have a maximum absolute difference with the Bloch-McConnell equations of $1.5 \cdot 10^{-3}$ which is not shown in these figures. These figures show the Bloch-McConnell fit as red dots and the spinlock fit as the blue line. Beneath these figures, the residual is shown which is defined as $S_{\text{Spinlock}} - S_{\text{BM simulation}}$.

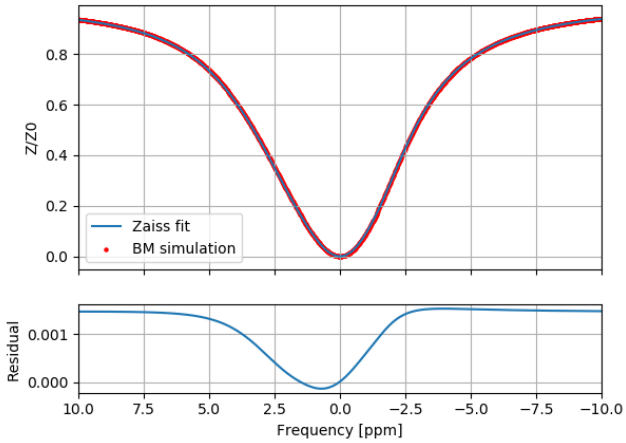

Figure 4.8: *The spinlock fit to Z-spectrum, the red dots depict the BM simulations and the blue line is the fit.*

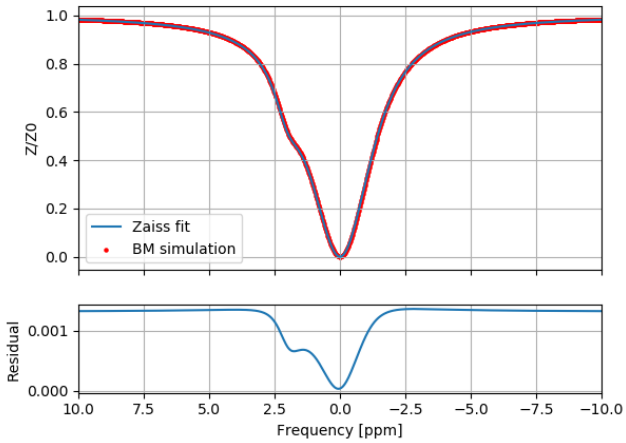

Figure 4.9: *The spinlock fit to Z-spectrum, the red dots depict the BM simulations and the blue line is the fit.*

4.2 Phantom Data

The 2-pool phantoms consist of glutamate or creatine solutions in purified water, with concentrations of $5mM$, $10mM$, $20mM$, $40mM$ and $80mM$. Figures 4.10 and 4.11 show the obtained Z-spectra of $10mM$ glutamate and $10mM$ creatine respectively.

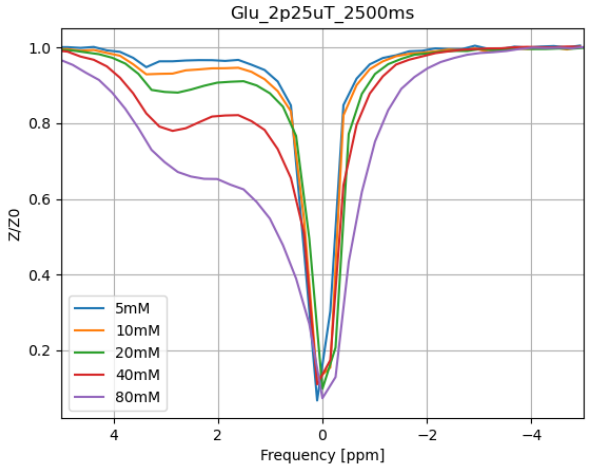

Figure 4.10: *Phantom measurement of glutamate with* $B_1 = 2.25\mu T$ *and* $t_{sat} = 2.5s$.

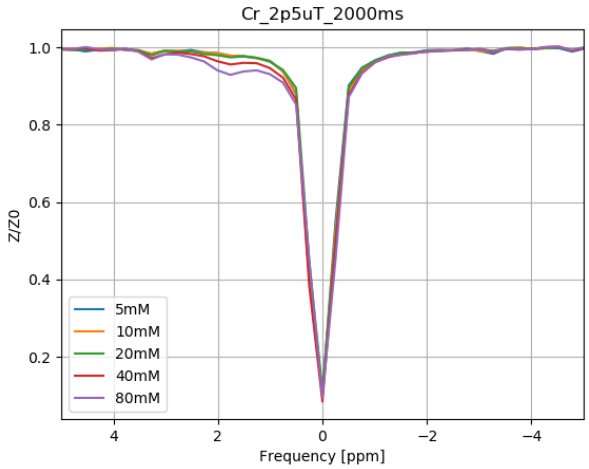

Figure 4.11: *Phantom measurement of creatine with* $B_1 = 2.5\mu T$ *and* $t_{sat} = 2s$.

Version of August 23, 2020– Created August 23, 2020 - 13:21

4.2.1 Optimize CEST Parameters for the Phantoms

For the phantoms, multiple measurements conducted for different B_1 values and saturation times were analyzed. The minimum value S_{phantom} around the dip at the chemical shift value of the target metabolite was saved in a matrix. These normalized matrices are shown for both metabolites at $10mM$, since they correspond most to the concentrations in the brain.

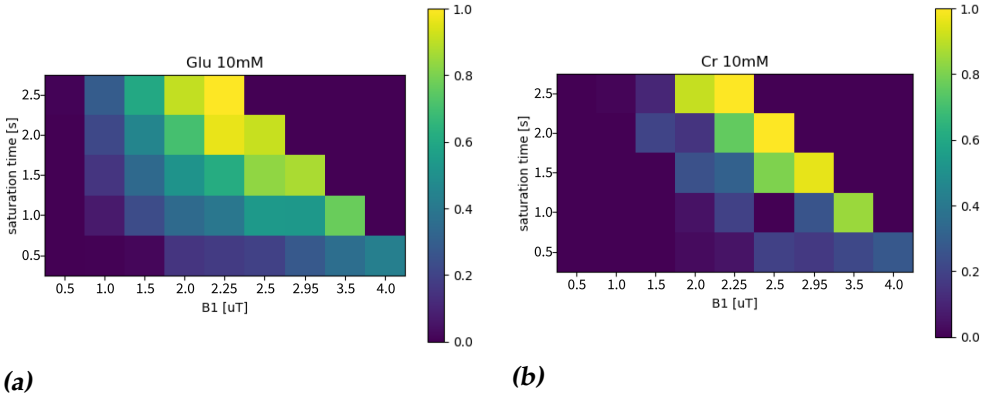

(a) ***(b)***

Figure 4.12: *The normalised optimisation matrices for glutamate (a) and creatine (b). The dark blue pixels in the upper right corner correspond to measurements that were not conducted due to SAR limitations.*

4.2.2 CEST Quantification Phantoms

For the Lorentzian fits, the spectrum was again plotted as $1 - Z$ just like with the Lorentzian fits of the Bloch-McConnell equations. The Lorentzian fits of the phantom data showed a maximum residual value of 0.29 for $B_1 = 0.5\mu T$ and $t_{sat} = 0.5s$. The figures (4.13 and 4.14) shown are fitted to the data of figures 4.10 and 4.11. To quantitatively compare the Lorentzian fits to the MTR asymmetry, figure 4.15 shows the obtained signal from the metabolite when using the respective method. For this figure, the height of the MTR asymmetry at the chemical shift was used to quantify the signal of the target metabolite and the amplitude of the Lorentzian was used for the Lorentzian signal.

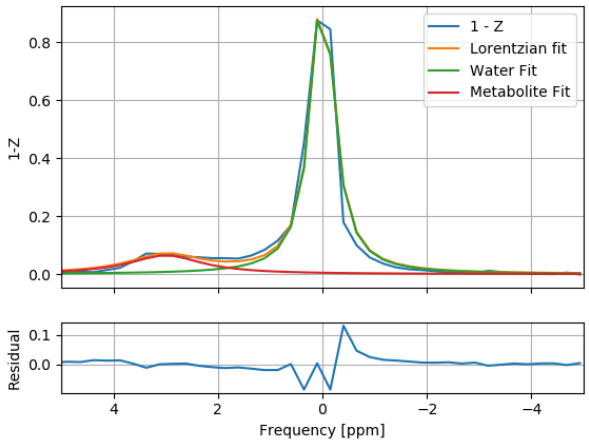

Figure 4.13: *Lorentzian fit of glutamate with* $B_1 = 2.25\mu T$ *and* $t_{sat} = 2.5s$.

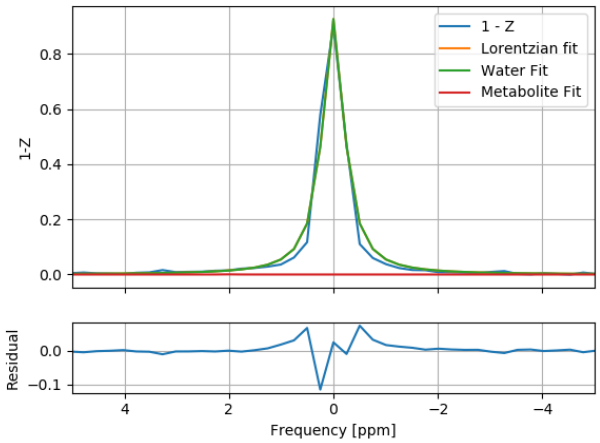

Figure 4.14: *Lorentzian fit of creatine with* $B_1 = 2.5\mu T$ *and* $t_{sat} = 2s$.

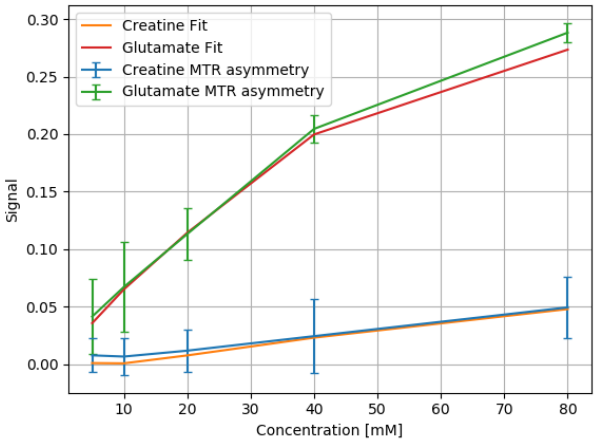

Figure 4.15: *The obtained signal from the MTR asymmetry versus the Lorentizan fits for both glutamate and creatine.*

4.2.3 Mixtures

To further test the Lorentzian fits, we made solutions of $10mM$ glutamate and $10mM$ creatine in purified water. For every B_1 and saturation time, the signal of the MTR asymmetry and the Lorentzian fit were compared. These matrices are shown in figure 4.16 for glutamate and figure 4.17 for creatine. Two examples for both glutamate and creatine can be found in figure 4.18 and 4.19.

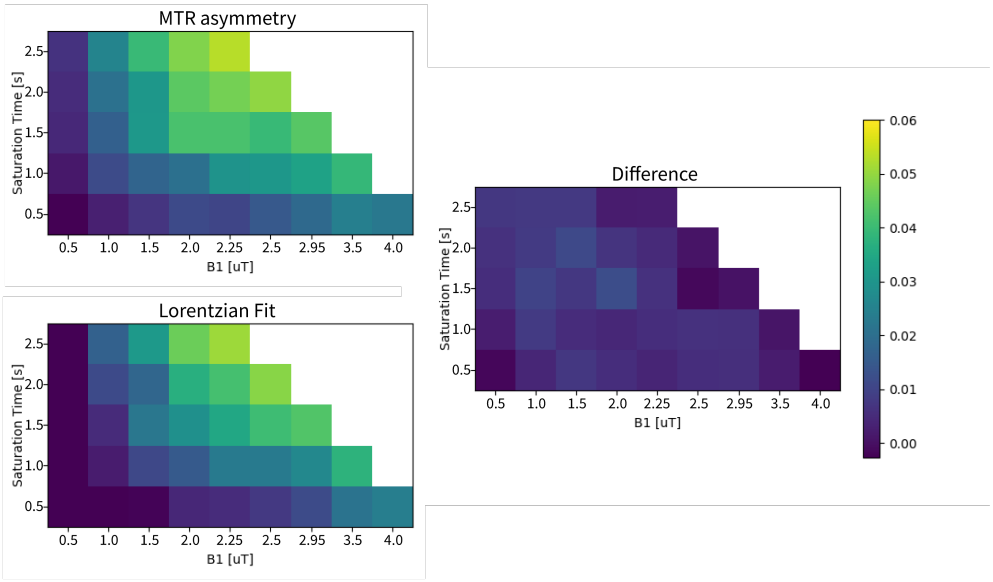

Figure 4.16: *Mixture phantom signal of glutamate from MTR asymmetry vs Lorentzian fit and the difference between the two. The highest value in the difference matrix is* 0.015.

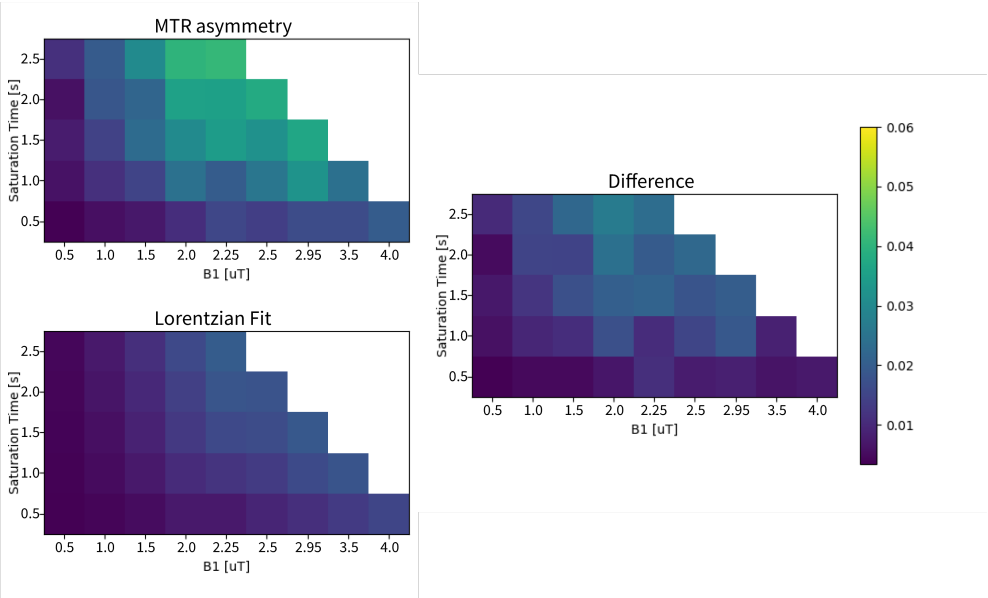

Figure 4.17: *Mixture phantom signal of creatine from MTR asymmetry vs Lorentzian fit and the difference between the two. The highest value in the difference matrix is* 0.03*.*

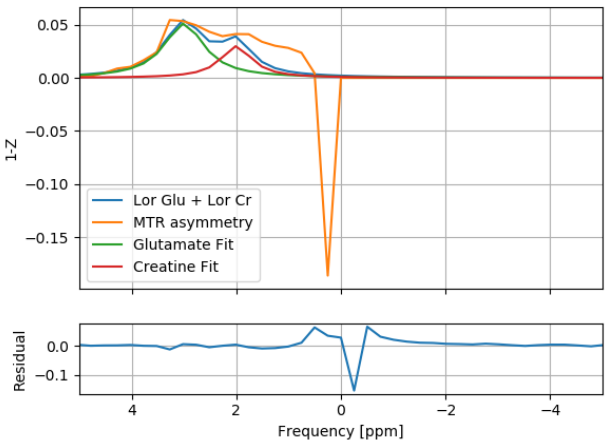

Figure 4.18: *The MTR asymmetry of the mixture phantom versus the Lorentzian fits, scan parameters were* $B_1 = 2.25\mu T$ *and* $t_{sat} = 2.5s$*.*

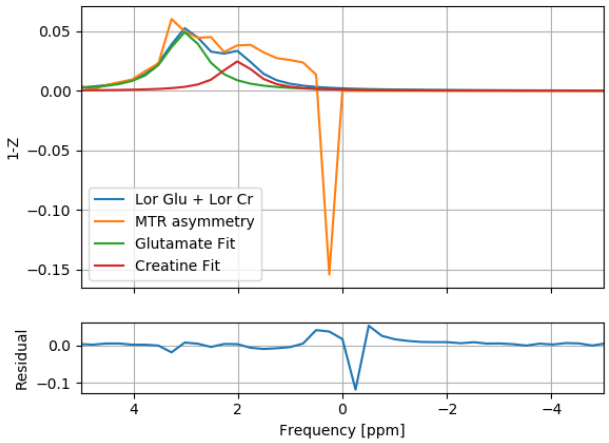

Figure 4.19: *The MTR asymmetry of the mixture phantom versus the Lorentzian fits, scan parameters were* $B_1 = 2.5\mu T$ *and* $t_{sat} = 2s$.

4.3 In Vivo Data

An In Vivo metabolite level map was only conducted for glutamate, which in literature is refered to as GluCEST. The signal in GluCEST is almost similarly defined as the MTR asymmetry, with the difference being the normalization:

$$\text{GluCEST} = \frac{Z(-\Delta\omega) - Z(\Delta\omega)}{Z(-\Delta\omega)} \quad . \tag{4.1}$$

In this equation, $\Delta\omega$ is the Larmor frequency of glutamate, which is $3ppm$. In the following figure (4.20), the GluCEST signal is calculated for every voxel. Furthermore, the average Z-spectrum is calculated for both the white matter and the grey matter separately (figure 4.21). Both the Lorentzian fit and the spinlock fit were fitted to the mean Z-spectra of grey and white matter. See figures 4.22 and 4.23 for the Lorentzian fits and figures 4.24 and 4.25 for the spinlock fits. The result of these fits are shown in table 4.1.

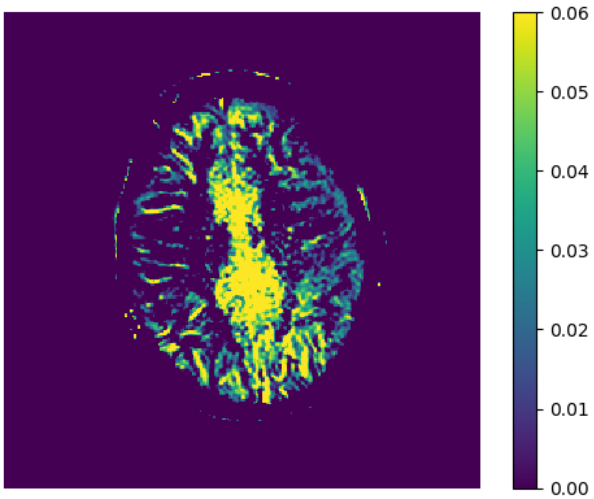

Figure 4.20: *The GluCEST image of a healthy volunteer, scan parameters were* $B_1 = 3.5\mu T$ *and* $t_{sat} = 1s$.

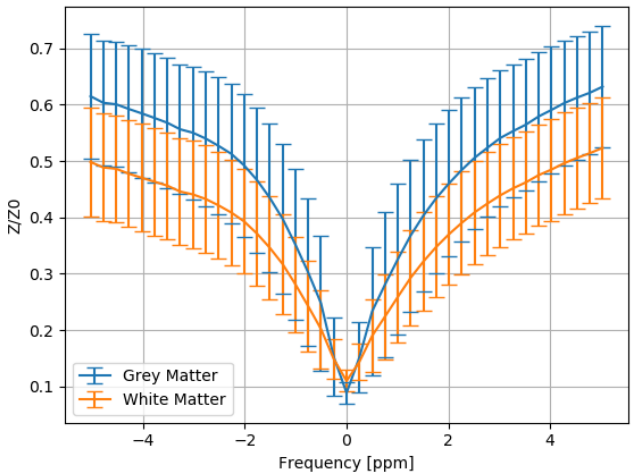

Figure 4.21: *The average Z-spectrum for Grey and White Matter.*

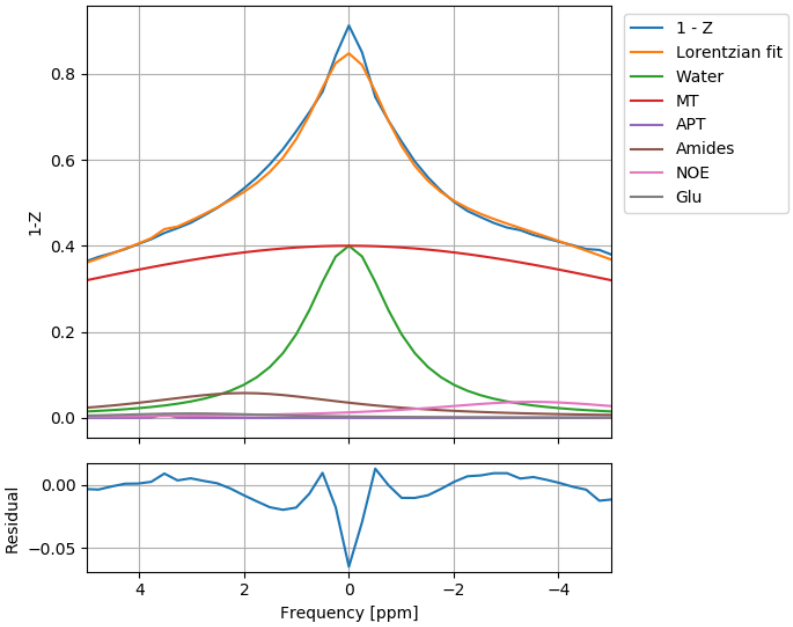

Figure 4.22: *Lorentzian fit to the mean grey matter Z-spectrum, the height of the glutamate Lorentzian is* $1 \cdot 10^{-10}$.

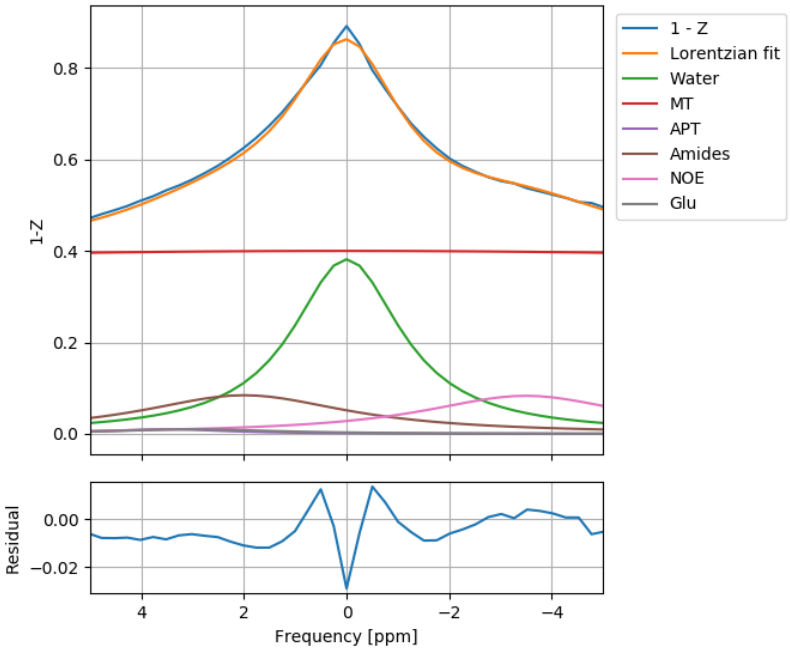

Figure 4.23: *Lorentzian fit to the mean white matter Z-spectrum, the height of the glutamate Lorentzian is* $1 \cdot 10^{-10}$.

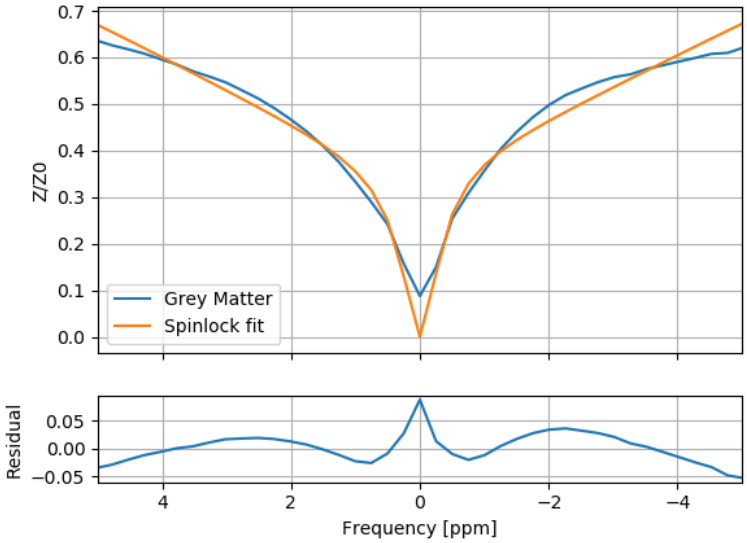

Figure 4.24: *Spinlock fit to the mean grey matter Z-spectrum.*

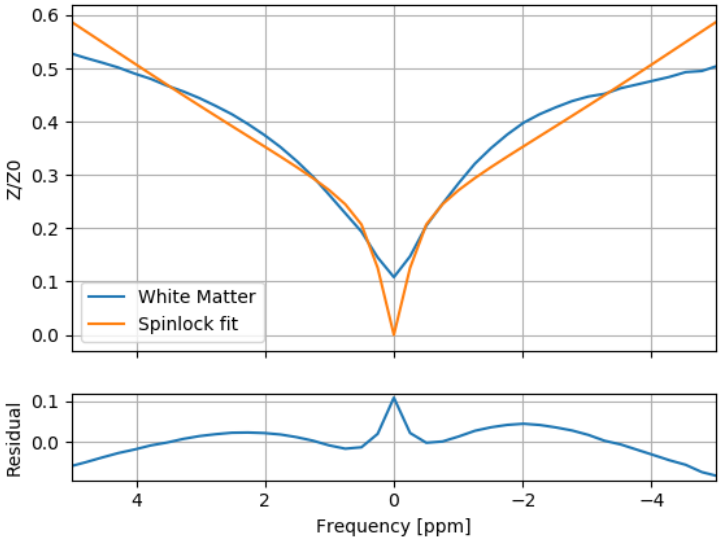

Figure 4.25: *Lorentzian fit to the mean white matter Z-spectrum.*

	Grey Matter	White Matter
MTR asymmetry	0.009 ± 0.023	0.002 ± 0.018
GluCEST	0.018 ± 0.044	0.001 ± 0.042
Lorentzian Fit	$1 \cdot 10^{-10}$	$1 \cdot 10^{-10}$
Spinlock Fit	0.020	$1.1 \cdot 10^{-16}$

Table 4.1: *The obtained signal from glutamate for every quantification method described in this thesis.*

5 Discussion

5.1 The Model used in the Simulations

The Bloch-McConnell simulation is based on a simplified n-pool model. Due to this simplification, it does not describe the physical system in detail. An example of this is that the model does not include different T_1 and T_2 for different tissues. For a very detailed model, one should include every pool, which is not numerically feasible. Furthermore, homogeneous B_1 is assumed, which is not the case in *in vivo* measurements. As all models, it is not complete, but it gives a good representation of CEST.

5.2 CEST Quantification

For the Bloch-McConnell simulation fits, Lorentzians showed to be less reliable than the spinlock fit by 2 orders of magnitude when comparing the residuals of both methods. The MTR asymmetry of the Bloch-McConnell simulation for glutamate is almost a factor 2 lower than the metabolite Lorentzian fit. This can be explained by the Lorentzian fitting method not being proposed for metabolite CEST, but for Amide Proton Transfer[15] (CEST focused on amides). The high residuals from the Lorentzians are not found for the spinlock fit which almost exactly corresponds to the Bloch-McConnell simulations. This is expected, since the spinlock fit is the eigenspace solution of the Bloch-McConnell equations.

For the phantom experiments, over the whole spectrum residuals, the Lorentzian fits seem to behave even worse. But those high residuals are only found around $0ppm$, not at the place of interest. At the value of the chemical shift of the target metabolite, the highest residual found is 0.05. When focusing on these parts of the spectrum (figure 4.15), the Lorentzian fits are shown to follow the same trend as the MTR asymmetry signal. In this figure, the signal for both the MTR asymmetry and the Lorentzian

fit at $80mM$ are lower than one would expect after the linear behaviour for 5-40mM. This may be caused by the glutamate chemical shift value shifting to $0ppm$ for higher concentrations, while the signal was collected at $3ppm$. After correcting for this shift, we expect to see linear behaviour, as is also found by Cai et al.[17].

In the mixtures, the Lorentzians also showed to be reliable at the chemical shift value of the target metabolite. The Lorentzian fits yield the same signal as the Lorentzian fits with a maximum difference of 0.015 for glutamate and 0.03 for creatine. This higher difference for creatine is explained from figures 4.18 and 4.19, the glutamate Lorentzian is broad and also has a significant amount of signal at $2ppm$. For this reason, the sum of both metabolite Lorentzians is also plotted to show that this sum does correspond to the MTR asymmetry. These figures also show that the MTR asymmetry obtained from a Z-spectrum that consists of multiple pools is less reliable for creatine than for glutamate.

The spinlock fit was not used for the phantoms because it uses metabolite properties (like exchange rate, T_2, etc.) from the brain. The brain properties do not correspond to the metabolite behaviour in the phantoms of water. This resulted in the spinlock fit looking very different from the phantom Z-spectrum. In an attempt to fix this by scanning a body temperature phantom, the casing used to keep the phantom warm yielded high B_1 inhomogeneity. This is the reason why the *in vivo* experiments were done at the optimal scan parameters found in the simulations instead of the phantoms.

5.3 In Vivo

The *in vivo* GluCEST image shows higher glutamate levels in grey matter than in white matter, which corresponds to GluCEST data found in literature[17][18]. Furthermore, the obtained optimal CEST parameters are close to the CEST parameters used by nanga et al. in their GluCEST paper[18].

The MTR asymmetry and the GluCEST yield high error values for both grey and white matter. This is due to the big differences between Z-spectra inside the grey and white matter which are caused by B_1 inhomogeneity. For both methods, the glutamate signal values were calculated for every voxel separately and a mean and standard deviation were obtained from these values.

The Lorentzian fits to the Grey and the White matter yield low residual that correspond to the residual values found in the phantoms. The differ-

ence here is that 6 Lorentzians were used for this fit, which corresponds to 12 fitting parameters (amplitude and FWHM for every Lorentzian). The NOE Lorentzian shows higher signal from NOE for white matter than for grey matter. White matter consists of a high amount of myelin[19], which yields a NOE effect. But the Lorentzians also show a high amount of signal from amides for both the grey matter and the white matter which is not expected in a healthy brain[4]. Furthermore, the Lorentzian fit shows almost no glutamate signal for the whole brain, which is incorrect. There may be 2 reasons for this error in the Lorentzian fits. First, the high amount of parameters may leave too much freedom for the fitting algorithm to interchange signal contribution. The other reason could be that the chemical shift of amides ($3.5ppm$) is too close to the chemical shift of glutamate ($3ppm$). These 2 challenges have to be solved for Lorentzian fitting to also become a viable method to separate signal in metabolite CEST.

The spinlock fit yields higher signal from glutamate in grey matter than in white matter, which is expected. Furthermore, the spinlock fit found the concentration of glutamate in grey matter to be $3mM$, where $\sim 9mM$ is expected. The main difference between the spinlock fit and the *in vivo* Z-spectra is the amount of water saturation. The spinlock fit assumes perfect water saturation, which is hard to achieve in real scans. For the spinlock fit to be viable, it has to be modified to also take non-perfect saturation into account.

5.4 Future Work

When modified to not always expect complete saturation of the water to fit better to *in vivo* Z-spectra, the spinlock fit shows potential. Since the spinlock fit uses the concentration of the CEST pools as a fitting parameter, it is able to show metabolite levels as a concentration. To be reliable in showing the concentrations, reference solutions need to be used. Without a reference solution, the method is just able to yield relative values for the metabolite amounts measured. The technique has to prove its reliability by comparison with established chemical composition methods like MRS and PET.

6 Conclusion

In this research, a metabolite simulation was constructed based on a 2-pool model which can be expanded to an n-pool model. Different quantification methods already used in CEST were described and tested for metabolite CEST. For phantom experiments, Lorentzian fits were shown to be reliable for metabolite CEST quantification. Optimal scan parameters obtained from the simulation were found to be $3.5\mu T$, $t_{sat} = 1s$ for glutamate and $2.95\mu T$, $t_{sat} = 1.5s$ for creatine. From the optimal scan parameters for glutamate, an acceptable GluCEST image was obtained, which could be further improved by B_1 inhomogeneity correction. The CEST signal from the *in vivo* experiments has shown to be hard to quantify, both the Lorentzian fit and the spinlock fit need to be adjusted and tested more to show their reliability.

6.1 Acknowledgements

During the research for this thesis, multiple things happened in my life. During these often hectic times, I could rely on Ece for giving me the time I needed. Furthermore, I appreciate that Ece always made time to help me with everything I needed for this research. Thanks to Bárbara Schmitz Abecassis for providing the grey and white matter mask for the *in vivo* experiments and for asking question during the journal club which made me understand the details of the presented paper even more. Also thanks to Jan-Willem and Lucia for the time they made in their schedules to watch my presentation and read this thesis.

Bibliography

[1] OECD (2020). Magnetic resonance imaging (mri) exams. *doi: 10.1787/1d89353f-en*, Accessed on 24 July 2020.

[2] OECD (2020). Magnetic resonance imaging (mri) units. *doi: 10.1787/1a72e7d1-en*, Accessed on 24 July 2020.

[3] William J. McEntee and Thomas H. Crook. Glutamate: its role in learning, memory, and the aging brain. *Psychopharmacology*, 111(4):391–401, July 1993.

[4] B. Wu, G. Warnock, M. Zaiss, C. Lin, M. Chen, Z. Zhou, L. Mu, D. Nanz, R. Tuura, and G. Delso. An overview of CEST MRI for non-MR physicists. *EJNMMI physics*, 3(1):19, December 2016.

[5] Frederic Martini, Judi Lindsley Nath, and Edwin F. Bartholomew. *Fundamentals of Anatomy & Physiology, Global Edition*, volume 10. Pearson, 2015.

[6] Joshua M. Tognarelli, Mahvish Dawood, Mohamed I.F. Shariff, Vijay P.B. Grover, Mary M.E. Crossey, I. Jane Cox, Simon D. Taylor-Robinson, and Mark J.W. McPhail. Magnetic Resonance Spectroscopy: Principles and Techniques: Lessons for Clinicians. *Journal of Clinical and Experimental Hepatology*, 5(4):320–328, December 2015.

[7] Feliks Kogan, Anup Singh, Catherine Debrosse, Mohammad Haris, Kejia Cai, Ravi Prakash Nanga, Mark Elliott, Hari Hariharan, and Ravinder Reddy. Imaging of glutamate in the spinal cord using GluCEST. *NeuroImage*, 77:262–267, August 2013.

[8] K. M Ward, A. H Aletras, and R. S Balaban. A New Class of Contrast Agents for MRI Based on Proton Chemical Exchange Dependent Saturation Transfer (CEST). *Journal of Magnetic Resonance*, 143(1):79–87, March 2000.

[9] Peter C. M. van Zijl, Wilfred W. Lam, Jiadi Xu, Linda Knutsson, and Greg J. Stanisz. Magnetization Transfer Contrast and Chemical Exchange Saturation Transfer MRI. Features and analysis of the field-dependent saturation spectrum. *NeuroImage*, 168:222–241, 2018.

[10] Donald E. Woessner, Shanrong Zhang, Matthew E. Merritt, and A. Dean Sherry. Numerical solution of the Bloch equations provides insights into the optimum design of PARACEST agents for MRI. *Magnetic Resonance in Medicine*, 53(4):790–799, 2005.

[11] Peter C. M. van Zijl and Nirbhay N. Yadav. Chemical exchange saturation transfer (CEST): what is in a name and what isn't? *Magnetic Resonance in Medicine*, 65(4):927–948, April 2011.

[12] Jinsuh Kim, Yin Wu, Yingkun Guo, Hairong Zheng, and Phillip Zhe Sun. A review of optimization and quantification techniques for chemical exchange saturation transfer MRI toward sensitive in vivo imaging. *Contrast Media & Molecular Imaging*, 10(3):163–178, June 2015.

[13] Moritz Zaiss and Peter Bachert. Chemical exchange saturation transfer (CEST) and MR Z-spectroscopy in vivo: a review of theoretical approaches and methods. *Physics in Medicine and Biology*, 58(22):R221–269, November 2013.

[14] Moritz Zaiss, Zhongliang Zu, Junzhong Xu, Patrick Schuenke, Daniel F. Gochberg, John C. Gore, Mark E. Ladd, and Peter Bachert. A combined analytical solution for chemical exchange saturation transfer and semi-solid magnetization transfer. *NMR in biomedicine*, 28(2):217–230, February 2015.

[15] Moritz Zaiss, Benjamin Schmitt, and Peter Bachert. Quantitative separation of CEST effect from magnetization transfer and spillover effects by Lorentzian-line-fit analysis of z-spectra. *Journal of Magnetic Resonance (San Diego, Calif.: 1997)*, 211(2):149–155, August 2011.

[16] Moritz Zaiss and Peter Bachert. Exchange-dependent relaxation in the rotating frame for slow and intermediate exchange – modeling off-resonant spin-lock and chemical exchange saturation transfer. *NMR in biomedicine*, 26(5):507–518, May 2013.

[17] Kejia Cai, Mohammad Haris, Anup Singh, Feliks Kogan, Joel H. Greenberg, Hari Hariharan, John A. Detre, and Ravinder Reddy. Magnetic Resonance Imaging of Glutamate. *Nature medicine*, 18(2):302–306, January 2012.

[18] Ravi Prakash Reddy Nanga, Catherine DeBrosse, Dushyant Kumar, David Roalf, Brendan McGeehan, Kevin D'Aquilla, Arijitt Borthakur,

Hari Hariharan, Damodara Reddy, Mark Elliott, John A. Detre, Cynthia Neill Epperson, and Ravinder Reddy. Reproducibility of 2D GluCEST in healthy human volunteers at 7 T. *Magnetic Resonance in Medicine*, 80(5):2033–2039, 2018.

[19] Marjo S. van der Knaap and Jacob Valk. *Myelin and White Matter*. Springer, Berlin, Heidelberg, 1995.